2016-07-01

The Virtual Source Approach to Non-Linear Potential Flow Simulations

Graham, David

http://hdl.handle.net/10026.1/6508

The Virtual Source Approach to Non-Linear Potential Flow Simulations

Kurt Langfeld [a], David I. Graham [a], Deborah M. Greaves [b], Arshad Mehmood [a], and Tim Reis [a]
[a] School of Computing, Electronics and Mathematics, Plymouth University, UK
[b] School of Marine Science and Engineering, Plymouth University, UK

ABSTRACT

In this paper, we develop the Virtual Source Method for simulation of incompressible and irrotational fluid flows. The method is based upon the integral equations derived by using Green's identity with Laplace's equation for the velocity potential. The velocity potential within the fluid domain is completely determined by the potential on a virtual boundary located above the fluid. This avoids the need to evaluate singular integrals. Furthermore, the solution method developed here is meshless in space in that discretisation is in terms of the spectral components of the solution along this virtual boundary. These are determined by specifying non-linear boundary conditions on the velocity potential on the air/water surface using Bernoulli's equation. A fourth-order Runge-Kutta procedure is used to update the spectral components in time. The method is used to model high-amplitude standing waves and sloshing. Results are compared with theory where applicable and some interesting physical phenomena are identified.

KEY WORDS: Nonlinear full potential flow, boundary integral equation, Green's function, meshless methods.

INTRODUCTION

In developing a comprehensive numerical wave tank (NWT), the approach of the authors and collaborators has been to couple together a number of distinct solvers, each serving a particular purpose depending upon the region of the numerical wave tank to be modelled. Near coastal structures or tethered devices, full Navier-Stokes solvers are required, possibly including the effects of compressibility. In the far-field region away from structures, however, a potential model will represent the flow adequately. Due to the overall complexity of the coupled NWT, each component must be computationally efficient. In a companion paper, a finite-volume model is developed to utilise the full capabilities of OpenFOAM® to solve the potential flow problem. Here, we use an integral equation approach.

Integral equation methods for solving water wave problems are very well established. In particular, the Boundary Element Method (BEM)

has been used frequently for a variety of wave-related problems. In the conventional BEM, the computation domain coincides with the physical fluid domain, requiring special treatment of the free surface and evaluation of certain singular integrals to evaluate flow quantities on the boundary. These singular integrals can be avoided, for example by using the de-singularised BEM approach (see e.g. Cao et al., (1991)). Other methods such as the Method of Fundamental Solutions (see Johnston and Fairweather (1984)) can also be developed to utilise the advantages of integral equation formulation (i.e. the reduction in spatial dimension) but without the need to evaluate singular integrals.

In the following, we outline the development of the Virtual Source Method and give details of how it is implemented in solving free surface problems. We then apply the method to both low-amplitude and high-amplitude standing waves. Results are compared and contrasted with second-order Airy solutions and interesting nonlinear effects are identified. Finally, we reflect upon the utility of the method and indicate further ares of development.
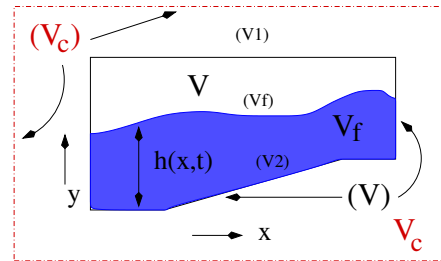
WAVE TANK GEOMETRY AND BOUNDARY CONDITIONS

Fig. 1 Wave tank geometry and definitions.

We will consider an incompressible fluid with vanishing viscosity that is confined to the volume V - the wave tank. The boundary of the volume V is denoted by (V) and consists of $(V1)$, the "ceiling", and $(V2)$, the

"walls" (see Fig. 1). The fluid surface is modelled by a function $h(x, t)$ with t being time. For later use, V_f is the volume occupied by the fluid and (V_f) denotes the free fluid surface. For the ease of the presentation, we here present the formulation for 2d scenarios only, but stress that the formulation van be straightforwardly extended to 3d simulations.

We assume that the flow is irrotational and can be described by the potential ϕ, which is related to the streaming velocity in the usual way ($\vec{x} = (x, y)$):

$$\vec{v}(\vec{x}, t) = \begin{pmatrix} u(\vec{x}, t) \\ w(\vec{x}, t) \end{pmatrix}, \quad \vec{v}(\vec{x}, t) = \vec{\nabla}\phi(\vec{x}, t). \tag{1}$$

Assuming further that the fluid is incompressible leads to a Laplace equation for the velocity potential:

$$\vec{\nabla} \cdot \vec{v} = 0 \quad \Rightarrow \quad \triangle\phi(\vec{x}, t) = 0 \text{ for } \vec{x} \in V_f. \tag{2}$$

For the virtual source approach, we extend the domain of validity from V_f to the volume of the entire wave tank V:

$$\triangle\phi(\vec{x}, t) = 0 \text{ for } (x, y) \in V. \tag{3}$$

At the "walls", i.e., $\vec{x} = (x, y) \in (V_2)$, we demand that the streaming velocity perpendicular to the wall vanishes:

$$\vec{n}(\vec{x}) \cdot \vec{\nabla}\phi(\vec{x}, t) = 0 \quad \text{for} \quad \forall \vec{x} \in (V2), \forall t, \tag{4}$$

where $\vec{n}(\vec{x})$ is the surface normal vector at point $\vec{x} \in (V2)$ (pointing from the inside of V to the outside). The free surface motion described by $h(\vec{x} \in (Vf), t)$ is obtained from Bernoulli's equation:

$$\frac{\partial}{\partial t}\phi(\vec{x}, t) = -g\, y - \frac{1}{2}\vec{\nabla}\phi(\vec{x}, t) \cdot \vec{\nabla}\phi(\vec{x}, t) \quad \vec{x} \in (V_f), \tag{5}$$

where we have set the atmospheric pressure at the surface to zero. $g = 9.81 m/s^2$ is the gravitational acceleration.

In order to introduce dimensionless variables, we choose appropriate length and time scales, leading to:

$$x = L_x\, \bar{x}, \quad y = L_y\, \bar{y}, \quad t = \sqrt{L_y/g}\,\bar{t},$$

$$u = \sqrt{g\, L_y}\frac{L_y}{L_x}\bar{u}, \quad v = \sqrt{g\, L_y}\bar{v}, \tag{6}$$

$$\phi = \sqrt{g\, L_y^3}\,\bar{\phi}.$$

The Bernoulli equation (5) then becomes

$$\frac{\partial\bar{\phi}}{\partial\bar{t}} = -\bar{y} - \frac{1}{2}\left[\kappa^2\bar{u}^2 + \bar{v}^2\right], \quad \kappa = \frac{L_y}{L_x}. \tag{7}$$

The function $h(x, t)$, which captures the free surface, is determined by the conservation of fluid mass (in dimensionless variables):

$$\frac{\partial\bar{h}}{\partial\bar{t}} = -\kappa^2\bar{u}\frac{\partial\bar{h}}{\partial\bar{x}} + \bar{v}(\vec{x}, t). \tag{8}$$

THE VIRTUAL SOURCE APPROACH

Any Green function to the Laplace operator defined on the volume B satisfies the equation

$$\triangle G(\vec{x}, \vec{x}_0) = -\delta(\vec{x} - \vec{x}_0), \tag{9}$$

but is only uniquely specified if boundary conditions have been specified for the boundary (B). A closed form for the Green function is available if we choose (for 3 dimensions)

$$B = \mathbb{R}^3, \quad \lim_{r \to \infty} G = 0, \quad G(\vec{x}) = \frac{1}{4\pi}\frac{1}{|\vec{x} - \vec{x}_0|}. \tag{10}$$

A common choice for 2 dimensions is

$$G(\vec{x}, \vec{x}_0) = -\frac{1}{2\pi}\log\big(|\vec{x} - \vec{x}_0|\big). \tag{11}$$

We stress that the choice above is for technical convenience only, i.e., the Green function is known in closed form. The choice does not reflect the boundary conditions (4,5) of the wave tank problem at all. Actually, a key-point of our method below is to take into account some of the boundary conditions already at Green function level.

The Boundary Element Method (BEM) (see e.g. Grilli et al., (1989)) starts with the choice of the fluid volume V_f for the volume B:

$$\phi(\vec{x}_0) = \int_{(V_f)}\left[G\,\vec{\nabla}\phi - \phi\,\vec{\nabla}G\right] \cdot d\vec{a} \quad \text{(BEM)} \tag{12}$$

The potential ϕ and its gradient $\vec{\nabla}\phi$ at the boundary (V_f) are the unknown quantities that are chosen such that the physical relevant boundary conditions (4) and (5) are satisfied. Since the Green function (as well its gradient) is singular for $\vec{x} \to \vec{x}_0$, this task requires a careful Garlekin discretisation of $\phi(\vec{x} \in (V_f))$ as well as some analytic integration. Note also that not only the time dependence is encoded by the free surface boundary condition (5), but also by a time dependent domain V_f of integration. Over the years, a wealth of sophisticated methods have been developed for this purpose (see e.g. Harris et al., (2014) for recent progress).

By contrast, for the *virtual source method* (VSM) we choose the volume $B = V_c$ with the fluid volume being a true subset of V_c (see Fig. 1 for an illustration), i.e.,

$$\phi(\vec{x}_0) = \int_{(V_c)}\left[G\,\vec{\nabla}\phi - \phi\,\vec{\nabla}G\right] \cdot d\vec{a} \quad \text{(VSM)} \tag{13}$$

$$V_f \subset V_c, \quad |\vec{x} - \vec{x}_0| > 0 \,\forall(\vec{x}, \vec{x}_0) \text{ with } \vec{x} \in V_c, \vec{x}_0 \in V_f. \tag{14}$$

This approach is similar to that used in de-singularised boundary element methods (see, Cao et al., (1991)). The advantages of these methods when compared to the standard BEM are twofold:

- The domain of integration, i.e. (V_c), is independent of time.
- The integral over the boundary in (13) is free of singularities by virtue of the regularising property of (14). This allows straightforward discretisation of the solution at the surface, and standard numerical integration schemes can be applied.

The VSM is further developed in the following section to derive a more tailored expression for the Green function than those used in Eqs. (10) or (11). Furthermore, the variables in the solution will be chosen to be wavenumber components of the solution along the virtual boundary, rather than field variables at collocation points.

Green function optimisation

The boundary element approach and the virtual source method (VSM) of the previous section employs the rather ad-hoc choice of the Green function (10) and (11) for the sake of the "closed expression" disregarding wave tank boundary conditions at Green function level. Here, we will give up the analytic closed form, and we will use the Green function with incorporated boundary conditions. We seek a Green function with

$$G(\vec{x}, \vec{x}_0)\Big|_{x \in (V1)} = 0, \quad \vec{n}(\vec{x}) \cdot \nabla G(\vec{x}, \vec{x}_0)\Big|_{x \in (V2)} = 0. \tag{15}$$

We now choose $B = V$ with $(B) = (V1) + (V2)$ and Green's identity reduces to

$$\int_{(V)}\left[\phi\,\triangle G - \triangle\phi\,G\right]d^3x = \int_{(V1)+(V2)}\phi\,\vec{\nabla}G \cdot d\vec{a} = \int_{(V1)}\phi\,\vec{\nabla}G \cdot d\vec{a}. \tag{16}$$

The latter equality holds because of our choice in (15). We observe that the velocity potential is now given entirely in terms of the potential at the top of the domain V:

$$\phi(\vec{x}_0, t) = -\int_{(V1)} \phi(\vec{x}, t)\vec{\nabla}G(\vec{x}, \vec{x}_0) \cdot d\vec{a} = -\int_{(V1)} \phi(\vec{x}, t)K(\vec{x}, \vec{x}_0)da \quad (17)$$

with the kernel

$$K(\vec{x}, \vec{x}_0) = \vec{\nabla}G(\vec{x}, \vec{x}_0) \cdot \vec{n}(\vec{x}), \quad \vec{n} : \text{surface normal vector.} \quad (18)$$

Using a rectangular wave tank with length L_x in x-directions and L_y in y direction, a short calculation yields (in the following we replace $\vec{x}_0 \rightarrow \vec{x}$):

$$\phi(\vec{x}, t) = \frac{2}{L_y} \sum_{nm} \frac{(-1)^{m+1} q_m}{k_n^2 + q_m^2} \sigma_n(t) \cos(k_n x) \cos(q_m y), \quad (19)$$

$$k_n = \frac{\pi}{L_x} n, q_m = \frac{\pi}{L_y} (m - 1/2), \quad n, m \in \mathbb{N},$$

where $\sigma_n(t)$ is the nth component of the Fourier cosine transform of the velocity potential along the virtual boundary ($V2$).

It turns out that omitting the mode $n = 0$ only changes ϕ by a homogeneous function of time that does not affect observables, i.e., the velocities u and v. We therefore may drop this contribution in the following. The sum over m can be analytically performed. We obtain:

$$\phi(\vec{x}, t) = \sum_{n \in \mathbb{N}} \sigma_n(t) \cos(k_n x) F\left(\frac{L_y}{L_x} n, \frac{y}{L_y}\right), \quad (20)$$

$$F(k, \bar{y}) = \sum_{\nu=0}^{\infty} (-1)^\nu \left[e^{-\pi k(2\nu+1+\bar{y})} + e^{-\pi k(2\nu+1-\bar{y})}\right], \quad k > 0. \quad (21)$$

The function F consists of an alternating sum with rapidly vanishing terms. It can be therefore numerically evaluated in a rapid and reliable way.

Implementation of the Virtual Source Method

In the following, we briefly introduce the numerical scheme to determine the time dependence of the virtual source components $\sigma_n(t)$ of the representation (5) and of the free surface $h(\vec{x}, t)$. In either case, we aspire to a high level time integration scheme, and will illustrate our approach using Runge-Kutta 4.

Virtual source evolution

Let us study the source evolution via (5) first. We discretise by replacing the infinite sum over all n in Eq. (20) by a finite sum of N_c components:

$$\phi(\vec{x}, t) \approx \sum_{n=1}^{N_c} \sigma_n(t) \cos(k_n x) F\left(\frac{L_y}{L_x} n, \frac{y}{L_y}\right). \quad (22)$$

Note that spatial derivatives, i.e., velocities, are known analytically at any point in space and time (mesh-free):

$$\vec{\nabla} \phi(\vec{x}, t) \approx \sum_{n=1}^{N_c} \sigma_n(t) \vec{\nabla}\left[\cos(k_n x) F\left(\frac{L_y}{L_x} n, \frac{y}{L_y}\right)\right]. \quad (23)$$

The Bernoulli Eq. (5) can then be written as

$$\frac{\partial}{\partial t} \phi(\vec{x}, t) = -g h(\vec{x}^{(s)}, t) - \frac{1}{2} \vec{\nabla}\phi(\vec{x}, t) \cdot \vec{\nabla}\phi(\vec{x}, t) = F\left(\vec{x}^{(s)}, h(\vec{x}^{(s)}, t), \sigma_n(t)\right),$$

where $\vec{x} \in V_f$ points to the fluid surface and $\vec{x}^{(s)}$ ignores the corresponding z-elevation: $\vec{x} = (x, y, h)^T \implies \vec{x}^{(s)} = (x, y)^T$, so that

$$\sum_{n=1}^{N_c} \frac{d\sigma_n(t)}{dt} K(k_n, \vec{x}) = -F\left(\vec{x}^{(s)}, h(\vec{x}^{(s)}, t), \sigma_n(t)\right). \quad (24)$$

Our aim is now to calculate the time derivatives $d\sigma_n/dt$ that will then be subjected to a Runge-Kutta 4 integration method. To this aim, we choose a set of points at the $\vec{x}_i^{(s)}$, $i = 1 \ldots N$ with $N \geq N_c$. Evaluating (24) at this set of points, we find:

$$\sum_{n=1}^{N_c} \frac{d\sigma_n(t)}{dt} K\left(k_n, (\vec{x}_i^{(s)}, h)^T\right) = -F\left(\vec{x}_i^{(s)}, h(\vec{x}_i^{(s)}, t), \sigma_n(t)\right), \quad i = 1 \ldots N. \quad (25)$$

The latter equation is a (potentially overdetermined) linear system to find the derivatives $d\sigma_n/dt$. In this paper, we obtain the optimal solution of this system by using Householder transformations.

We also need the time derivatives dh/dt in order to make the Runge-Kutta integration complete. We will here study two different implementations for solving the surface evolution via (8): a finite difference scheme and a Fourier decomposition of the surface elevation h.

Finite difference scheme

This is the most straightforward scheme: for any set of sources at time t, i.e., $\sigma_n(t)$, the velocities u and w in (1) are known analytically (see (23)). With the set of points $\vec{x}_i^{(s)}$, $i = 1 \ldots N$ already needed for the calculation of $d\sigma/dt$ (see last subsection), confine us to solve for the set

$$h_i(t) = h\left(\vec{x}_i^{(s)}, t\right). \quad (26)$$

To ease the notation, we consider the 2-dimensional case where the points $\vec{x}_i^{(s)}$ are aligned on the x-axis. We obtain an approximation of the derivative $\partial h/\partial x$ in (8), by a centred difference:

$$\frac{\partial}{\partial t} h(x_i, t) \approx \frac{h_{i+1}(t) - h_{i-1}(t)}{x_{i+1} - x_{i-1}}. \quad (27)$$

The evolution Eq. (8) takes the form

$$\frac{dh_i(t)}{dt} = G\left(\vec{x}_i^{(s)}, \sigma_n(t), h_i(t)\right). \quad (28)$$

Assume that $\sigma_n(t)$ and $h_i(t)$ are known for a given time t. The solution of the Eqs. (25) and (28) then yields the derivatives dh_i/dt and $d\sigma_n/dt$ which can subsequently be used for the Runge-Kutta 4 integration.

Airy mode decomposition

Rather than discretising h using the grid points $x_i^{(s)}$, we perform a Fourier expansion of the spatial dependence:

$$h(x, t) = \sum_{k=0}^{N_A} \left[a_k(t) \cos\left(\frac{2\pi}{L_x} k\, x\right) + b_k(t) \sin\left(\frac{2\pi}{L_x} k\, x\right)\right]. \quad (29)$$

If the Fourier coefficients h_k^A possess a harmonic time dependence, (29) would represent the Airy perturbative solution. We therefore call the representation (29) *Airy mode decomposition*. For moderate wave steepness, we therefore expect that only a small number of modes are significantly different from zero.

With the decomposition (29), the spatial derivative is known analytically

$$\frac{\partial}{\partial x} h(x, t) = \frac{2\pi}{L_x} \sum_{k=0}^{N_A} \left[-a_k(t) \sin\left(\frac{2\pi}{L_x} k\, x\right) + b_k(t) \cos\left(\frac{2\pi}{L_x} k\, x\right)\right]. \quad (30)$$

The surface evolution Eq. (8) then takes the form

$$\sum_{k=0}^{N_A}\left[\frac{da_k(t)}{dt} \cos\left(\frac{2\pi}{L_x} k\, x\right) + \frac{db_k(t)}{dt} \sin\left(\frac{2\pi}{L_x} k\, x\right)\right] = H\left(x, a_k(t), b_\ell(t), \sigma_n(t)\right). \quad (31)$$
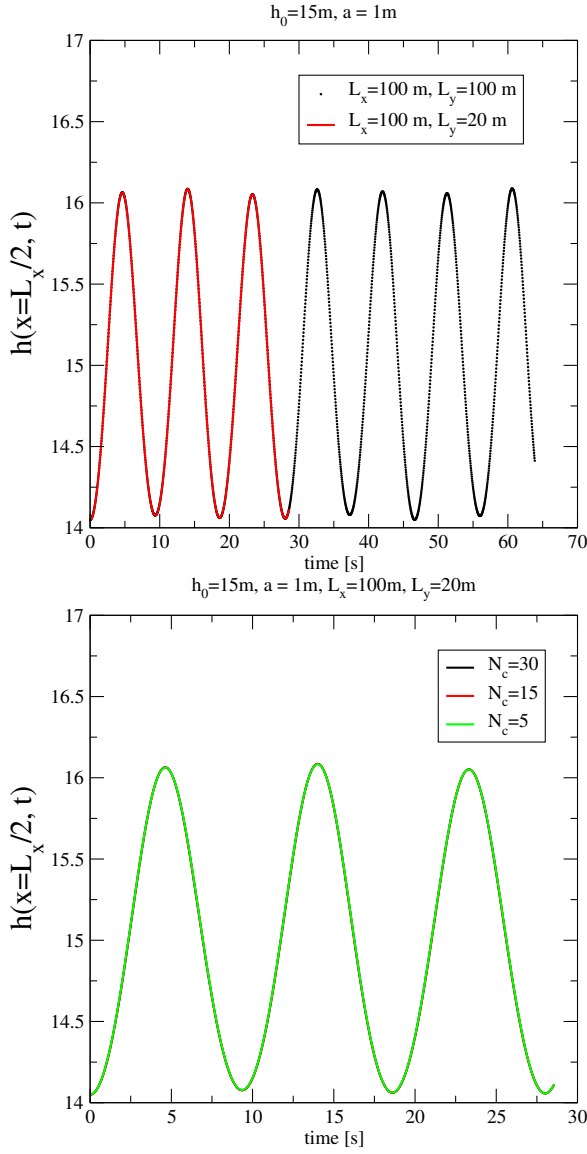
Fig. 2 Top: wave height $h(L_x/2, t)$ as a function of time t for two wave tank geometries: $(L_x, L_y) = (100m, 100m)$ and $(L_x, L_y) = (100m, 20m)$. Bottom: result for several numbers N_c of virtual sources.

Choosing a set of $N_s \geq 2N_A$ points for x, the latter system can be solved again using Householder optimisation. Inverse discrete Fourier transform is, of coures, a viable alternative. In summary, for any given coefficients $a_k(t)$, $b_k(t)$ and $\sigma_n(t)$ at time t, the Householder solution yields the derivatives

$$\frac{da_k(t)}{dt}, \quad \frac{db_\ell(t)}{dt}, \quad \frac{d\sigma_n(t)}{dt} \tag{32}$$

needed for the Runge-Kutta integration.

TESTING

We test our VSM formulation for a standing wave scenario for which we expect that the 2nd order Airy solution is a good approximation: the length of the tank is $L_x = 100$m, the calm water surface is at $h_0 = 15$m and the initial wave amplitude is given by $a = 1$m. The initial fluid

configuration is at rest, i.e., $\vec{v}(\vec{x}, t = 0) = 0$. The profile of the water column $h(x, t = 0)$ is set to the second order Airy solution for the standing wave, $h(x, t = 0) = h_A(x, 0)$ with

$$h_A(x, t) = h_0 + a \cos(kx) \cos(\omega t) + \frac{\pi a^2}{L_x} \left[\cos^2(\omega t) \right.$$
$$\left. - \frac{1}{4 \cosh^2(kh_0)} + \frac{3}{4 \sinh^2(kh_0)} \cos(2\omega t) \right] \cos(2kx). \tag{33}$$
$$c^2 = \frac{gL_x}{2\pi} \tanh(kh_0), \quad T = \frac{L_x}{c}, \quad \omega = \frac{2\pi}{T}, \quad k = \frac{2\pi}{L_x}. \tag{34}$$

Our numerical result must be independent of the extent L_y of the wave tank container as long as $h(x, t) < L_y \forall x, t$. This, however, provides a non-trivial test for our formulation since the ratio L_y, L_x is manifestly present in e.g. (20) of our method. The reason for this is that the Green function strongly depends on the domain, i.e., the tank container. We have numerically studied the mid wave height $h(L_x/2, t)$ as a function of time t for two different tank geometries: $L_y = 100$m and $L_y = 20$m. We used $N_x = 50$ points for the resolution in x-direction, and $N_c = 15$ sources. We performed 2000 time steps with a fixed discretisation of $\delta \bar{t} = 0.01$. This means that a smaller physical time t is reached after the 2000 steps for the case $L_y = 20$m (see (6)). Our finding is shown in Fig. 2, top panel, and good agreement of both data sets is indeed observed.

The next step is to check convergence with respect to the number N_c of spectral components. The bottom panel of Fig. 2 compares the findings for the tank geometry $(L_x = 100m, L_y = 20m)$ for the cases of $N_c = 5, 15, 30$. We find that a few as $N_c = 5$ yields accurate results for the current case.

To study the effects from the discretisation of the x-coordinate, we keep $N_c = 15$ fixed and calculate the profile $h(x, t = T)$ after one periodic time T for a different number of points $N_x = 20, 50, 100$. The results are compared with the 2nd order Airy solution $h_A(x, T)$ (33) in Fig. 3, top panel. The agreement with Airy's solution is already good for $N_x = 20$.

We finally explore the convergence of the time integration. To this aim, we numerically calculate the surface profile $h(x_i, t)$, $i = 1 \ldots N_x$ for T/dt time integration steps. The data set with the smallest $dt = T/1250$ is taken as the reference set $h_r(x_i, T)$. Note that for $L_x = 100$m and $a = 1$m, the Airy expansion parameter ka is of order 0.06. This implies that we might see already higher order corrections beyond the 2nd order Airy expansion. If we aim to study the precision of the time integration beyond the 1% level, we cannot choose the Airy solution (33) as a reference. In order to quantify the error, we define:

$$\text{err}(dt) = \sqrt{\frac{1}{N_x} \sum_{i=1}^{N_x} \left[h(x_i, T) - h_r(x_i, T) \right]^2}. \tag{35}$$

Our numerical findings for this quantity as a function of dt is shown Fig. 3, bottom panel. We find that our data are consistent with a scaling of the error proportional to dt^4 thus confirming the 4th order level of our Runge-Kutta integration.

Extreme standing waves

As a first applications, we search for standing waves in the planar wave tank in the highly non-linear regime for which the ration between amplitude a and wavelength is not necessarily a small parameter. Note that only for a linearised surface evolutions Eq. (8), periodic solutions with a harmonic time dependence of ϕ and h are guaranteed. In the non-linear regime, the state of the wave tank might not return to the same initial profile $h(x, 0)$ with vanishing streaming velocities $u, v = 0$ everywhere.
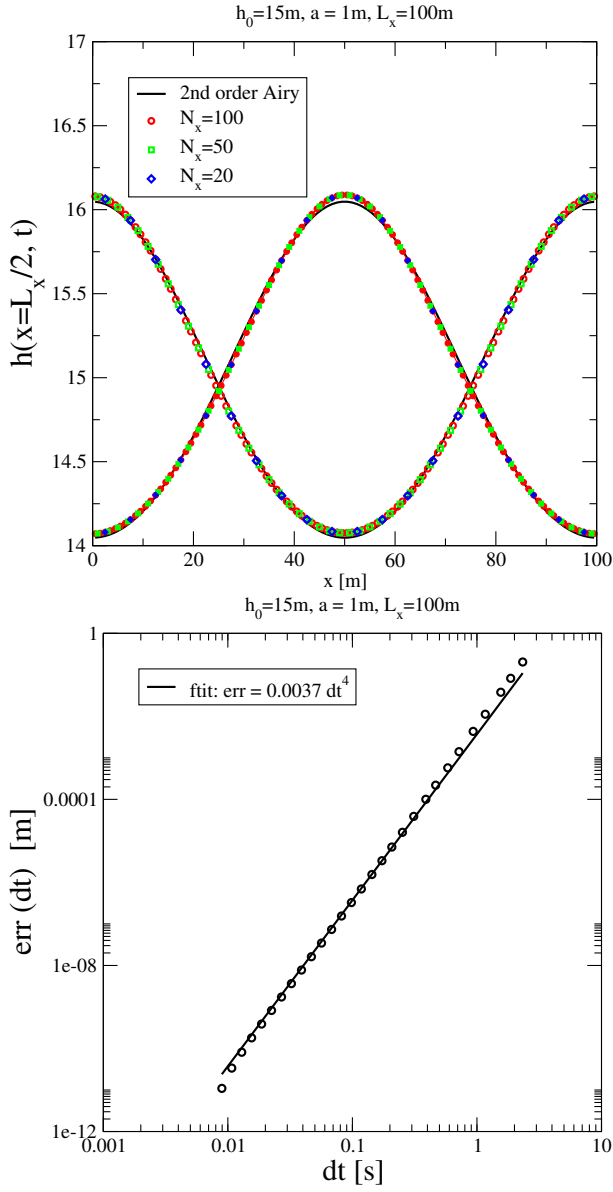
Fig. 3 Top: The wave profiles $h(x, T)$ and $h(x, 3T/2)$ after one periodic time t as a function of x for several numbers of points N_x used to discretise x. Bottom: The time integration error as function of the discretisation length dt.
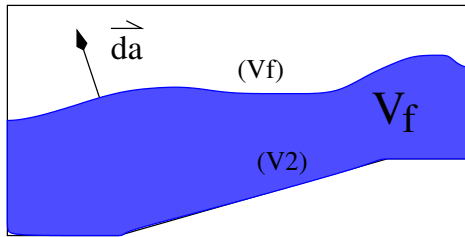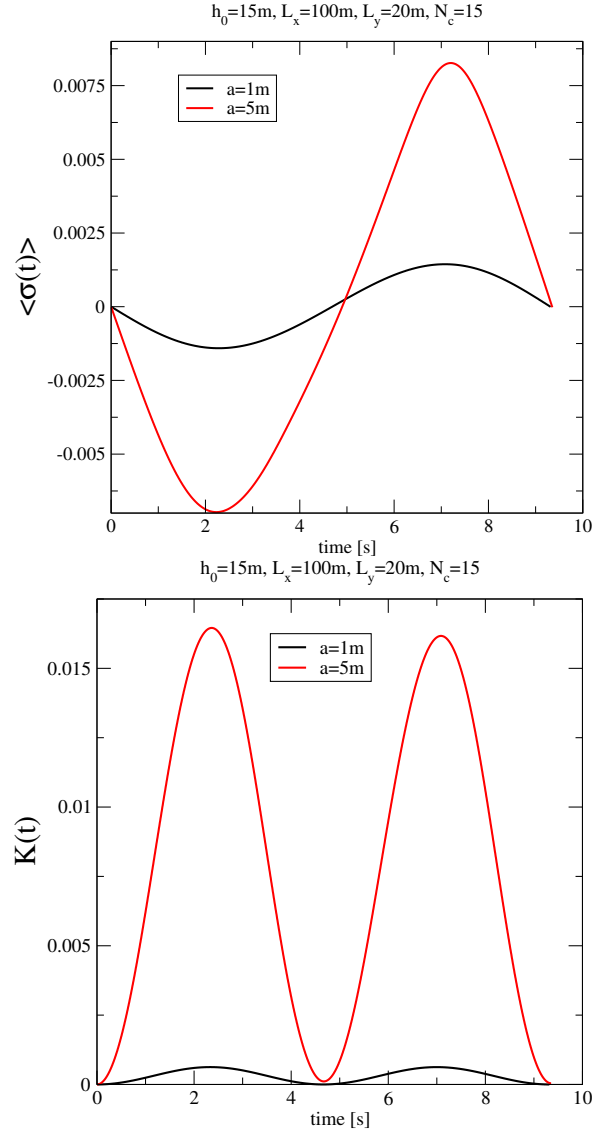

Fig. 4 Wave tank and surface elements.

Fig. 5 Top: The source average as a function of time t for two different initial amplitudes a. Bottom: the dimensionless kinetic energy $\bar{K}(t)$.

In such a non-linear setting, we firstly need to define the period time T. To this aim, we introduce the "kinetic energy" of the fluid by

$$K(t) := \frac{\rho}{2} \int_{V_f} d^2x \, \vec{\nabla}\phi(\vec{x}, t) \, \vec{\nabla}\phi(\vec{x}, t) \qquad (36)$$

where the integration extends over the fluid volume V_f. Apparently, K is semi-positive quantity with $K(0) = 0$. Although we are not aware of any proof that the state of the fluid must return to the state of vanishing K after some time, we will present numerical evidence below that this indeed true for the cases considered here. We therefore define the periodic time T by

$$K(T) = 0, \quad K(t) \neq 0 \quad \forall 0 < t < T. \qquad (37)$$

Using that $\triangle\phi(\vec{x}, t) = 0$ for $\vec{x} \in V_f$, the kinetic energy can be expressed
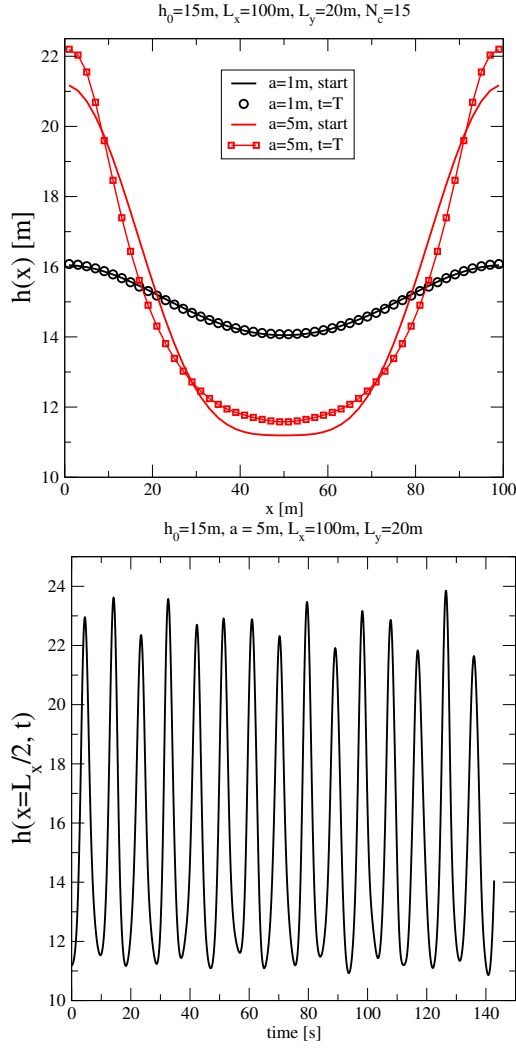
Fig. 6 Top: The surface profile after one pseudo-periodic time T.
Bottom: Long-term time evolution of the water height h at
$x = L_x/2$.

as a surface integral:

$$K(t) := \frac{\rho}{2} \int_{(V_f)} \phi(\vec{x}, t) \, \vec{\nabla}\phi(\vec{x}, t) \cdot d\vec{a}. \tag{38}$$

Note that

$$\vec{\nabla}\phi(\vec{x}, t) \cdot d\vec{a} = 0 \quad \forall \vec{x} \in \text{wall}, \tag{39}$$

and that the surface normal vector at the free surface is given by

$$d\vec{a} = \begin{pmatrix} -\partial h/\partial x \\ 1 \end{pmatrix} dx. \tag{40}$$

We therefore find:

$$K(t) = \frac{\rho}{2} \int \phi(\vec{x}, t) \left[-u\frac{\partial h}{\partial x} + v \right] dx. \tag{41}$$

We find this equation numerically most useful, but point out that the later equation can be written in compact form using (8):

$$K(t) = \frac{\rho}{2} \int \phi(\vec{x}, t) \frac{\partial h(\vec{x}, t)}{\partial t} dx. \tag{42}$$

In dimensionless units, we obtain:

$$K = \rho g L_y^2 L_x \bar{K}, \quad \bar{K} = \frac{1}{2} \int \bar{\phi}\left[-\kappa^2 \, \bar{u}\frac{\partial \bar{h}}{\partial \bar{x}} + \bar{v} \right] d\bar{x}. \tag{43}$$

Initially, the kinetic energy vanishes due to our choice $\sigma_n(t = 0) = 0, \forall n$. We define the source average

$$\langle \sigma(t) \rangle = \frac{1}{N_c} \sum_{i=1}^{N_c} \sigma_i(t). \tag{44}$$

From

$$\langle \sigma^2 \rangle \geq \langle \sigma \rangle^2 \tag{45}$$

it is clear that not all components σ_n can vanish if $\langle \sigma(t) \rangle \neq 0$. This implies that

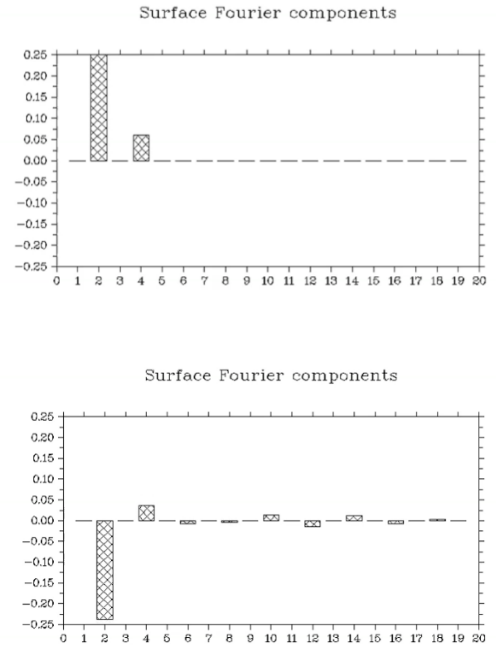$$K > 0 \quad \text{for} \quad \langle \sigma \rangle \neq 0. \tag{46}$$

Fig. 7 Development of higher harmonics for extreme standing
waves. Modes at $t = 0$ (top); Modes at $t = 10$ (bottom).

At $t = 0$, we start with 2nd order Airy solution (33), i.e., $h(x, 0) = h_A(x, 0)$. Fig. 5, top panel, shows that, at least for an amplitude $a = 1$m, the time dependence of $\langle \sigma(t) \rangle$ almost follows a harmonic function. Although shown is $\langle \sigma \rangle$ for $a = 5$m, for which we expect significant non-linearities. This is seen from our numerical result for this case that significantly deviates from a harmonic behaviour. In any case, for the investigation of a potentially periodic behaviour, only times T for which $\langle \sigma(T) \rangle = 0$ can qualify as "periodic time". We point out that the linear behaviour of $\langle \sigma(t) \rangle$ close to its zeros is numerically helpful to calculate T. At the same time, we numerically obtain the kinetic energy K. Only if $K(T)$ is satisfactorily close to zero, we call T a candidate for a periodic time. Fig. 5, bottom panel, shows the kinetic energy as a function of time t for the two cases $a = 1m$ and $a = 5m$. In both cases, the kinetic energy drops to a quite low value at $t = T$. For small amplitudes, e.g., $a = 1$m, we confirm that this initial surface profile is recovered to a good
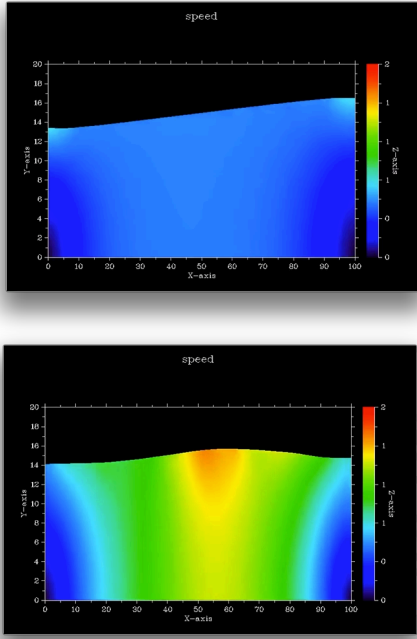
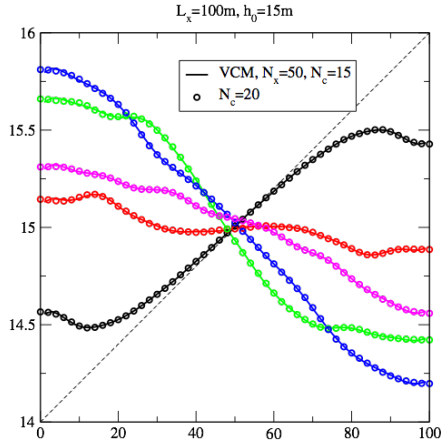Fig. 8 Water collapse: surface at $t = 0.1$ (top); surface at $t = 32$ (bottom).

Fig. 9 Comparison between free surface profiles for VSM with 15 (solid lines) or 20 (symbols) frequency components.

Sloshing

As a further example to demonstrate the effectiveness of the method when higher harmonics are present from the start of the computation, we investigate the collapse of a tilted free surface. The initial configuration is a tilted surface which is then free to deform under gravity. Two snapshots of the speed of the fluid fro two different times are shown in Fig. 8. In the present case of small initial slope, the solution is given as a superposition of Fourier modes of an infinite number of frequencies. However, the periods of the Fourier modes are not integer multiples of lower frequencies, meaning that the solution is not periodic. Fig. 9 shows that the VSM solution with $N_c = 15$ frequency components in the model agrees very well with the solution with $N_c = 20$ components small-amplitude case, demonstrating convergence in terms of the number of frequency components required.
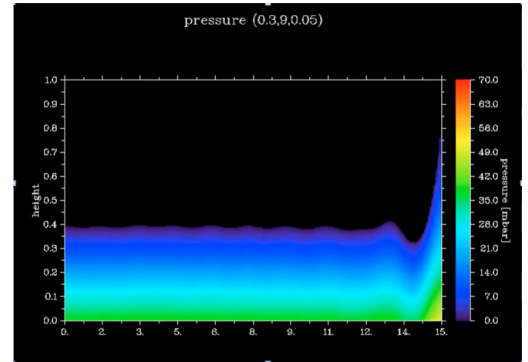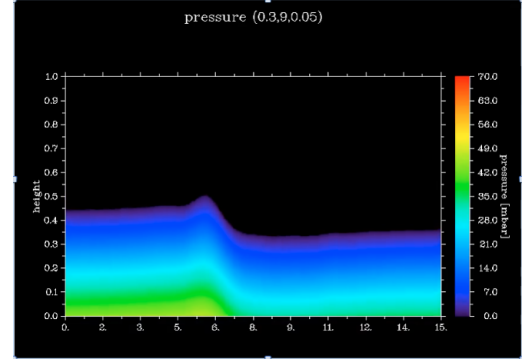

Fig. 10 Sloshing: developing surface (top); surface at impact (bottom).

extent (see Fig. 6, top panel). If the amplitudes are as big as $a = 5$m, the significant deviations from the start profile are observed, and the surface motion is not periodic at all. In the reminder of the section, we will explore whether we can tune the initial profile $h(x, 0)$ in such a way that it is restored after one periodic time t. Fig. 6, bottom panel, shows the long term time evolution of the water column h at $x = L_x/2$. Higher harmonics are clearly visible. This is even more evident in Fig. 7, where the magnitudes of the first twenty frequency components are plotted for an extreme standing wave (amplitude 5m in 15m deep water) at $t = 0$ and $t = 10$.
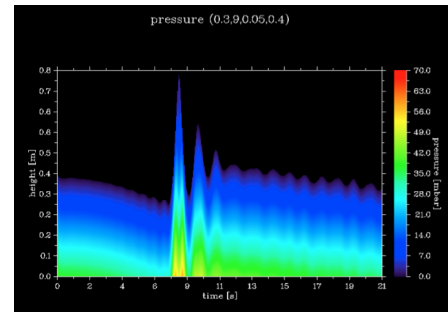

Fig. 11 Pressure oscillations after sloshing impact.

In a separate study of sloshing, we start with an equilibrate free water surface at time $t = 0$, i.e., $h(x, 0) =$ constant, at rest. We then apply a time-limited force in x-direction to the fluid, which is strongest at the left end of the wave tank. The presence of the force modifies the Bernoulli Eq. (5) to

$$\frac{\partial}{\partial t} \phi(\vec{x}, t) = -g\, y - \frac{1}{2}\, \vec{\nabla}\phi(\vec{x}, t) \cdot \vec{\nabla}\phi(\vec{x}, t) + \varphi(x)\, \exp\{-t^2/\tau^2\}, \qquad (47)$$

where $\varphi(x)$ is the integrated force profile and τ is the duration of the force pulse (details will be presented elsewhere). Note that the external force rapidly disappears with increasing time. Its role is to set the water in motion finally leading to a run-up of water at the right end of the wave tank. Fig. 10 shows the pressure distribution in the fluid at two different times, i.e., at the early stage of a propagating hump of water and at impact time on the right of the wave tank. In Fig. 11, we show the pressure distribution at the right end of the wave tank as a function of time. We clearly observe a spike at impact and a subsequent oscillation of the water column post impact.

3-D Simulations

Finally, we stress that our approach can be easily generalised to 3 dimensions. In this case, the Green function in (20,21) needs to be extended to cover the extra dimension and to incorporate a vanishing normal velocity at sea bed and surrounding walls. The virtual sources now form a 2-dimensional grid at the top of the wave tank $\sigma_n(t) \rightarrow \sigma_{nm}(t)$. We here only show our preliminary findings for a 3d standing wave. Fig. 12 show the speed of the fluid within the 3d wave tank at two different times. Details will be left to a future publication.

CONCLUSIONS

In this paper, we have developed and used a Virtual Source Method for solving free-surface potential flow problems. The method is meshfree in space, the only discretisation being in terms of the frequency components of the velocity potential along a virtual boundary away from the fluid domain. The method has been shown to be 4th-order accurate in time. By utilising the method for high-amplitude standing waves, nonlinear effects beyond second-order Airy theory can easily be identified. The method is well suited to inviscid sloshing and has been extended to three spatial dimensions. Future work will include development of the method to cope with progressive waves and wave interactions with solid structures.

ACKNOWLEDGMENTS

REFERENCES

Cao Y, Schulz, WW, Beck, RF (1991). "Three-dimensional desingularised boundary integral method for potential problems," *Intl J Numerical Methods in Fluids* , 12(8), 785-803.

Grilli, ST, Skourup, J. and Svendsen, IA (1989). "An Efficient Boundary Element Method for Nonlinear Water Waves", Engineering Analysis with Boundary Elements, 6(2), 97-107.

Harris, JC, Dombre, E, Benoit, M, and Grilli, ST (2014). "Fast Integral Equation Methods for Fully Nonlinear Water Wave Modeling," Proc 24th Int Offshore and Polar Eng Conf, Busan, Korea, June 15-20, 2014.

Johnston,RL, Fairweather,G (1984). "The Method of Fundamental Solutions for Problems in Potential Flow", *Applied Math. Modelling* 8, 265-270.
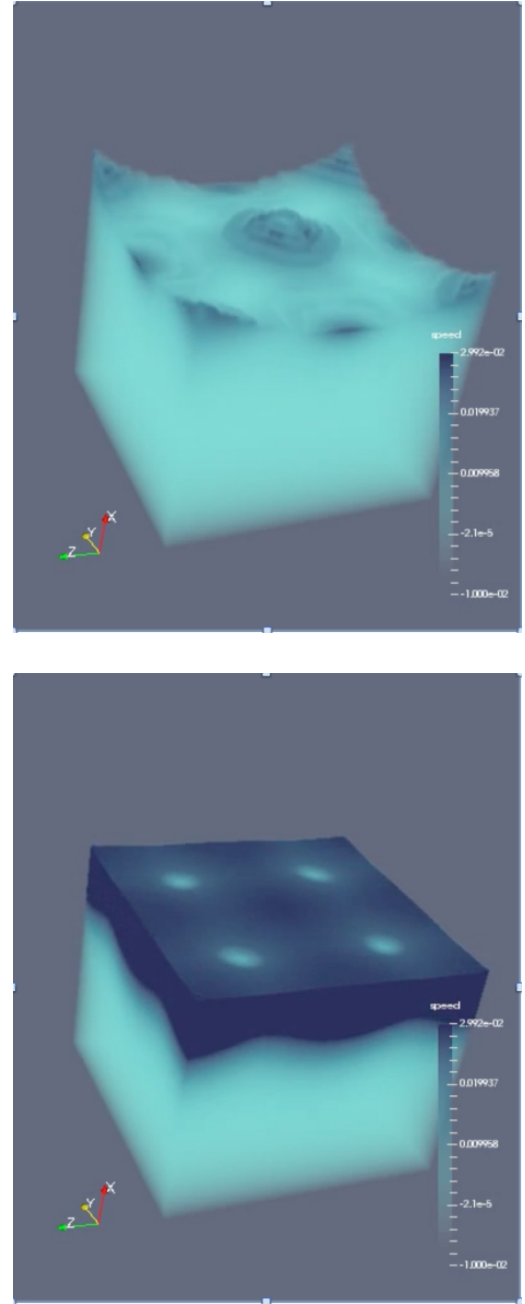
Fig. 12 3-D simulations: colour coding shows the speed of the fluid (dark: high speed); initial surface (top); surface at mid-period (bottom).